Redox signaling modulates Rho activity and tissue contractility in the *Caenorhabditis elegans* spermatheca

Charlotte A. Kelley[a], Sasha De Henau[b], Liam Bell[a], Tobias B. Dansen[b], and Erin J. Cram[a,*]
[a]Department of Biology, Northeastern University, Boston, MA 02115; [b]Center for Molecular Medicine, Molecular Cancer Research Section, University Medical Center Utrecht, Universiteitsweg 100, 3584 CG Utrecht, the Netherlands

ABSTRACT **Actomyosin-based contractility in smooth muscle and nonmuscle cells is regulated by signaling through the small GTPase Rho and by calcium-activated pathways. We use the myoepithelial cells of the *Caenorhabditis elegans* spermatheca to study the mechanisms of coordinated myosin activation in vivo. Here, we show that redox signaling modulates RHO-1/Rho activity in this contractile tissue. Exogenously added as well as endogenously generated hydrogen peroxide decreases spermathecal contractility by inhibition of RHO-1, which depends on a conserved cysteine in its nucleotide binding site (C20). Further, we identify an endogenous gradient of H_2O_2 across the spermathecal tissue, which depends on the activity of cytosolic superoxide dismutase, SOD-1. Collectively, we show that SOD-1-mediated H_2O_2 production regulates the redox environment and fine tunes Rho activity across the spermatheca through oxidation of RHO-1 C20.**

Monitoring Editor
Jeffrey Hardin
University of Wisconsin, Madison

Received: Apr 13, 2020
Accepted: Apr 28, 2020

INTRODUCTION

Coordinated cellular contractility is important for many biological processes, including shaping of tissues during morphogenesis (Mason *et al.*, 2013; Siedlik and Nelson, 2015) and proper function of contractile tissues, including those found in the intestine (Citalán-Madrid *et al.*, 2017; Hartl *et al.*, 2019), cardiovascular system (Smiesko and Johnson, 1993; Wettschureck and Offermanns, 2002; Pedrosa Nunes *et al.*, 2010), and respiratory systems (Gunst *et al.*, 2003; Smith *et al.*, 2003; Doeing and Solway, 2013). To study regulation of cell contractility in vivo, we use the *Caenorhabditis elegans* spermatheca, which is part of the hermaphroditic somatic gonad, as a model system. The somatic gonad is made up of two U-shaped gonad arms, in which germ cells and oocytes are surrounded by smooth muscle–like sheath cells (Strome, 1986; McCarter *et al.*, 1997; Hubbard and Greenstein, 2000). The spermatheca, the site of fertilization, consists of 24 myoepithelial cells and is connected to the uterus by a four-cell syncytium called the spermatheca–uterine (sp-ut) valve (Strome, 1986; McCarter *et al.*, 1997, 1999; Hubbard and Greenstein, 2000; Gissendanner *et al.*, 2008).

Successful ovulation into, and transit through, the spermatheca requires the coordination of spermathecal contractility. Upon oocyte entry into the spermatheca, the distal cells of the spermatheca and sp-ut valve contract to keep the newly fertilized embryo in the spermatheca (Tan and Zaidel-Bar, 2015; Kelley *et al.*, 2018) while the eggshell forms (Maruyama *et al.*, 2007). After a regulated period of time, the distal spermatheca contracts while the sp-ut valve relaxes, resulting in expulsion of the embryo into the uterus (McCarter *et al.*, 1999). When this process is misregulated, embryos can become trapped in the spermatheca (Bui and Sternberg, 2002; Kariya *et al.*, 2004; Kovacevic and Cram, 2010; Kovacevic *et al.*, 2013; Wirshing and Cram, 2017, 2018; Kelley *et al.*, 2018) or be pushed prematurely into the uterus and become misshapen or damaged (Norman *et al.*, 2005; Kovacevic and Cram, 2010; Tan and Zaidel-Bar, 2015; Kelley *et al.*, 2018; Bouffard *et al.*, 2019).

As in smooth muscle and nonmuscle cells, phosphorylation of myosin drives contraction of the spermatheca (Sellers, 1981; Conti and Adelstein, 2008; Vicente-Manzanares *et al.*, 2009; Wirshing and Cram, 2017). In the spermatheca, two parallel pathways act to activate myosin. In one, the phospholipase PLC-1/PLCε (Kariya *et al.*, 2004; Kovacevic *et al.*, 2013) triggers ITR-1/IP_3 receptor-dependent calcium release and activation of the myosin light-chain kinase

This article was published online ahead of print in MBoC in Press (http://www.molbiolcell.org/cgi/doi/10.1091/mbc.E20-04-0236) on May 6, 2020.

*Address correspondence to: Erin J. Cram (e.cram@northeastern.edu).

Abbreviations used: F-actin, filamentous actin; GFP, green fluorescent protein; RNAi, RNA interference; ROCK, Rho kinase; ROS, reactive oxygen species; sp-ut, spermatheca–uterine valve.

MLCK-1 (Pilipiuk *et al.*, 2009; Kovacevic *et al.*, 2013; Kelley *et al.*, 2018). In the second, the RhoGAP SPV-1 is displaced from the membrane upon oocyte entry, allowing activation of the small GTPase RHO-1/Rho (Tan and Zaidel-Bar, 2015). This results in activation of LET-502/ROCK (Wissmann *et al.*, 1997, 1999; Tan and Zaidel-Bar, 2015), which, in addition to phosphorylating myosin directly (Amano *et al.*, 1997; Totsukawa *et al.*, 2004; Gally *et al.*, 2009; Beach *et al.*, 2017), inactivates the myosin phosphatase, MEL-11 (Kimura *et al.*, 1996; Wissmann *et al.*, 1999). While both of these pathways increase cell contractility, spatial differences have been observed. MLCK-1 is expressed throughout the spermathecal bag (Kelley *et al.*, 2018). LET-502/ROCK is expressed at higher levels in the distal cells of the spermatheca and sp-ut valve than in the central cells of the spermatheca and plays an important role in coordinating the entry of the oocyte and the onset of the exit of the fertilized embryo (Tan and Zaidel-Bar, 2015; Kelley *et al.*, 2018).

Although reactive oxygen species (ROS) can damage cells through covalent modification of lipids, proteins, and DNA (Birben *et al.*, 2012; Schieber and Chandel, 2014), ROS, in the form of hydrogen peroxide (H_2O_2), can also play important regulatory roles at physiological levels (Biswas *et al.*, 2006; Finkel, 2011; Xu *et al.*, 2017), including regulating contractility (Heo and Campbell, 2005; Clempus and Griendling, 2006; Aghajanian *et al.*, 2009; San Martin and Griendling, 2010; Xu and Chisholm, 2014; Horn *et al.*, 2017; Xu *et al.*, 2017). Intracellular ROS are produced primarily by complexes I and III of the mitochondrial electron transport chain (Grivennikova and Vinogradov, 2006; Bleier and Dröse, 2013; Wong *et al.*, 2017) and by NADPH oxidases (NOX; Bedard *et al.*, 2007) in the form of superoxide. Superoxide dismutases (SOD) catalyze the conversion of superoxide to hydrogen peroxide (H_2O_2; Fukai and Ushio-Fukai, 2011), a more long-lived oxidant and the second messenger in redox signaling (Dickinson and Chang, 2011). *C. elegans* expresses two cytosolic superoxide dismutases, SOD-1 and SOD-5 (Braeckman *et al.*, 2016). SOD-1 is more widely expressed in the adult than SOD-5 and acts in the cytosol and the mitochondrial intermembrane space (Doonan *et al.*, 2008; Yanase *et al.*, 2009; Braeckman *et al.*, 2016).

H_2O_2 can signal by reversible modification of specific solvent-exposed cysteines. Cysteine thiols (R-SH) that are deprotonated to thiolate anions ($R\text{-}S^-$) can be oxidized to a sulfenic group (R-SOH), which can condense with a nearby cysteine thiol to form a disulfide (R-S-S-R), reduced back to the original state, or further oxidized, which tends to be damaging (Biswas *et al.*, 2006; Finkel, 2011). Several in vitro (Heo and Campbell, 2005; Heo *et al.*, 2006) and in vivo (Gerhard *et al.*, 2003; Aghajanian *et al.*, 2009; Xu and Chisholm, 2014; Horn *et al.*, 2017) studies have shown that RhoA is redox-sensitive. Oxidation of Rho can lead to increased activity, either by enhancing nucleotide exchange or by alteration of GAP and GEF activity (Heo and Campbell, 2005; Aghajanian *et al.*, 2009; Horn *et al.*, 2017). Other studies have shown that oxidation of the conserved cysteine (C20) results in disulfide bond formation with the adjacent cysteine (C16), thereby blocking GTP loading (Gerhard *et al.*, 2003; Heo *et al.*, 2006; Mitchell *et al.*, 2013; Xu and Chisholm, 2014) and deactivating Rho. It is likely that whether oxidation of Rho leads to its activation or inhibition depends on the select oxidant used (Heo and Campbell, 2005; Heo *et al.*, 2006).

Here, we asked if H_2O_2 plays a role in the coordinated contractility of the *C. elegans* spermatheca. We found that exogenous H_2O_2 inhibits myosin activation through oxidation of RHO-1, leading to a subsequent loss of contractility in the spermatheca. Furthermore, we show that there are spatial differences in H_2O_2 across the tissue, and that this gradient is mediated in part by SOD-1, a cytosolic superoxide dismutase. Together, our data suggest that enzymes that regulate H_2O_2 can modulate the spatial redox environment and contractility across a tissue.

RESULTS

Exogenous hydrogen peroxide inhibits spermathecal contractility

Ovulation of an oocyte into the spermatheca and subsequent expulsion of the fertilized embryo into the uterus require coordination of the contractility of cells between the sheath, spermatheca, and sp-ut valve (Tan and Zaidel-Bar, 2015; Wirshing and Cram, 2017; Kelley *et al.*, 2018; Kelley and Cram, 2019). Entry requires coordination between the sheath cells and the distal spermathecal cells (McCarter *et al.*, 1997; Lints and Hall, 2009) and begins when the distal neck cells open. We refer to the time from distal neck dilation until entry of the oocyte into the spermatheca and neck closure as the "entry time" (Figure 1A). Upon entry, the oocyte is fertilized, and the eggshell begins to form. We refer to the time during which the embryo is completely surrounded by the spermathecal tissue as the "dwell time." During the dwell time, the distal neck cells and sp-ut valve contract to prevent both reflux of the embryo into the oviduct and premature exit of the embryo into the uterus. During embryo exit, the sp-ut valve relaxes, while the distal and central cells of the spermatheca contract to expel the embryo into the uterus. We refer to the time from the moment the sp-ut valve begins to open until full expulsion of the embryo into the uterus as the "exit time" (Figure 1A).

To determine if redox signaling might play a role in regulating ovulation or transit of embryos through the spermatheca, we first treated animals with exogenous H_2O_2 and examined overall tissue response using time-lapse DIC microscopy. *C. elegans* are fed *Escherichia coli*. However, *E. coli* metabolize H_2O_2, resulting in a reduction in H_2O_2 concentration. To prevent this, we used a modified *E. coli* strain JI377 (ΔahpCF katG katE) and compared it with the otherwise isogeneic strain MG1655 (wild-type *E. coli*; Seaver and Imlay, 2001). MG1655 expresses catalases and peroxidases and rapidly degrades H_2O_2. JI377 lacks two catalases and an alkyl hydroperoxide reductase and does not degrade H_2O_2 (Seaver and Imlay, 2001). We placed nematodes on plates seeded with either of the two strains, supplemented or not with 1 mM H_2O_2 and monitored ovulations after 45 min. While entry time was not affected by H_2O_2 treatment (Figure 1B, comparing 1 mM H_2O_2 + JI377 with the other three conditions), animals exposed to H_2O_2 had shorter dwell times and longer exit times than those not treated with H_2O_2 (Figure 1, C and D, comparing 1 mM H_2O_2 + JI377 with the other three conditions). Because no significant differences were observed between unsupplemented plates with either bacterial strain, for subsequent experiments we used MG1655 on plain NGM plates as our untreated control (referred to as untreated or $-H_2O_2$). We also took time-lapse movies of wild-type animals treated with a more stable peroxide analog, *tert*-butyl hydroperoxide (An *et al.*, 2005). Similarly to the effects seen with H_2O_2 treatment, 45-min pretreatment with 1 mM *tert*-butyl hydroperoxide results in shorter dwell times and longer exit times, while there was no significant difference in entry time (Figure 1, E–G). These results suggest that oxidation results in a shortened time the embryo spends in the spermatheca.

To determine if exogenously applied H_2O_2 leads to increased levels of H_2O_2 within the spermatheca, we expressed the ratiometric GFP-based probe roGFP2::TSA2ΔC$_R$, localized to the outer mitochondrial membrane via the targeting sequence from TOMM-20 (Wiedemann *et al.*, 2004; Gutscher *et al.*, 2009; Morgan *et al.*, 2016). This sensor is specifically oxidized by H_2O_2 and is similar to a

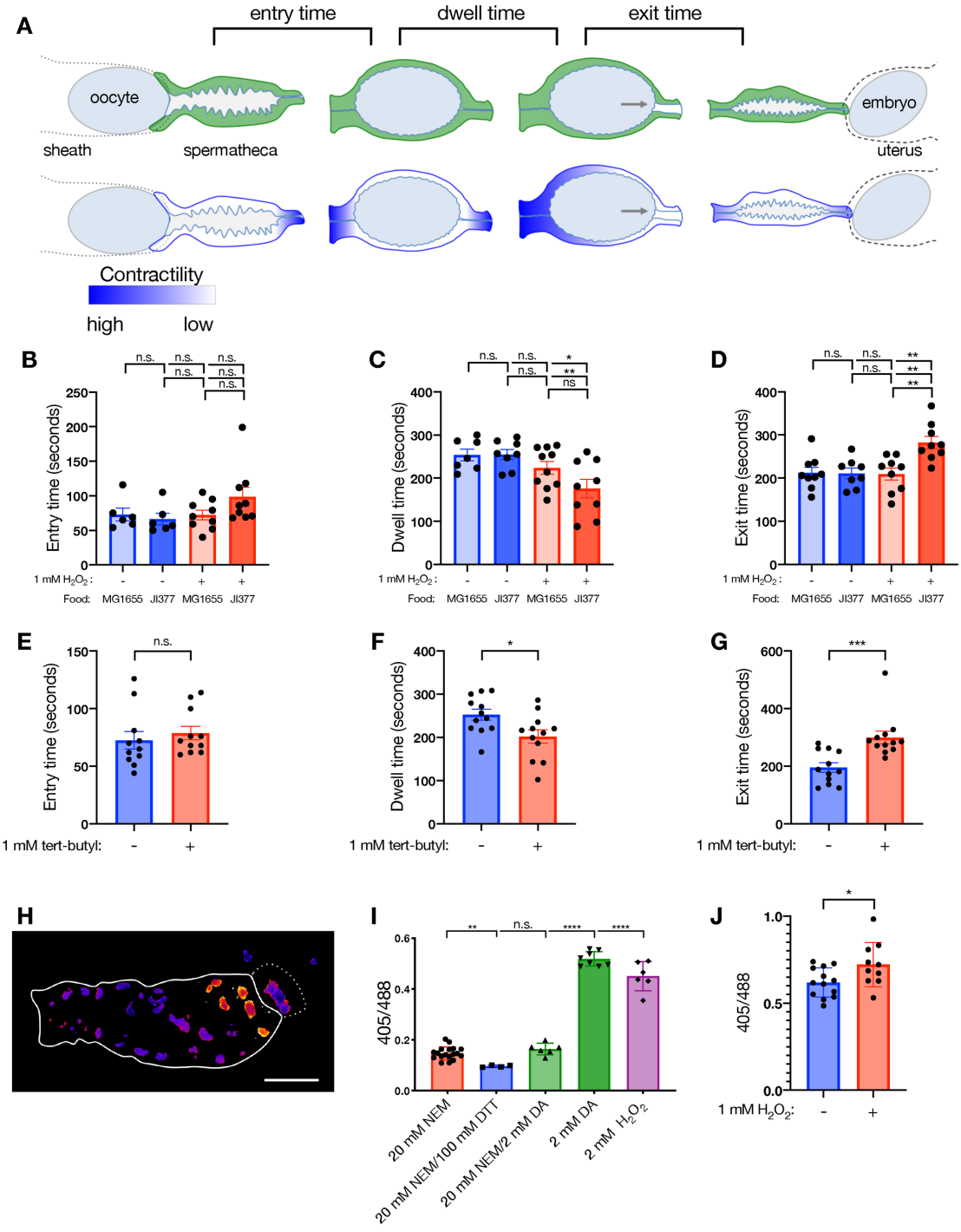

FIGURE 1: Exogenous hydrogen peroxide treatment affects spermatheca tissue contractility and oocyte transit. (A) Diagram of oocyte transit through the spermatheca, illustrating the transit metrics (top panel) and which regions of the spermatheca must contract to allow proper timing and direction of ovulation (bottom panel). (B) No significant change in entry time is observed with or without H_2O_2 treatment (+H_2O_2 seeded with JI377 bacteria, –H_2O_2 seeded with K12, - H_2O_2 seeded with JI377, or + H_2O_2 seeded with MG1655). Treatment with H_2O_2 (+H_2O_2 seeded with JI377 bacteria) results in shorter dwell times (C) and slower exit times (D) than all other conditions. Each point represents a time measurement taken from a single first ovulation. Error bars are SEM. One-way ANOVA with Tukey's multiple comparisons: ns $p > 0.05$, * $p \leq 0.05$, ** $p \leq 0.01$. Treatment with 1 mM tert-butyl hydroperoxide before imaging results in no difference in entry time (E), shorter dwell times (F) and longer exit times (G). Each point represents a time measurement calculated from a single, first ovulation. Error bars are SEM. Unpaired *t* test: * $p \leq 0.05$. (H) Representative image of a dissected spermatheca treated with NEM before fixation and imaging. Scale bar 20 μm. (I) Quantification of 405/488 ratio for animals treated with NEM or oxidants or reducing agents. Each point represents the average 405/488 of an entire spermatheca treated with the given agent before fixation and imaging. Error bars are SEM. Unpaired *t* test: ns $p > 0.05$, ** $p \leq 0.01$, *** $p \leq 0.001$, **** $p \leq 0.0001$. (J) Quantification of 405/488 ratio in live animals imaged either with no H_2O_2 or on slides supplemented with 1 mM H_2O_2. Error bars are SEM. Unpaired *t* test: * $p \leq 0.05$.

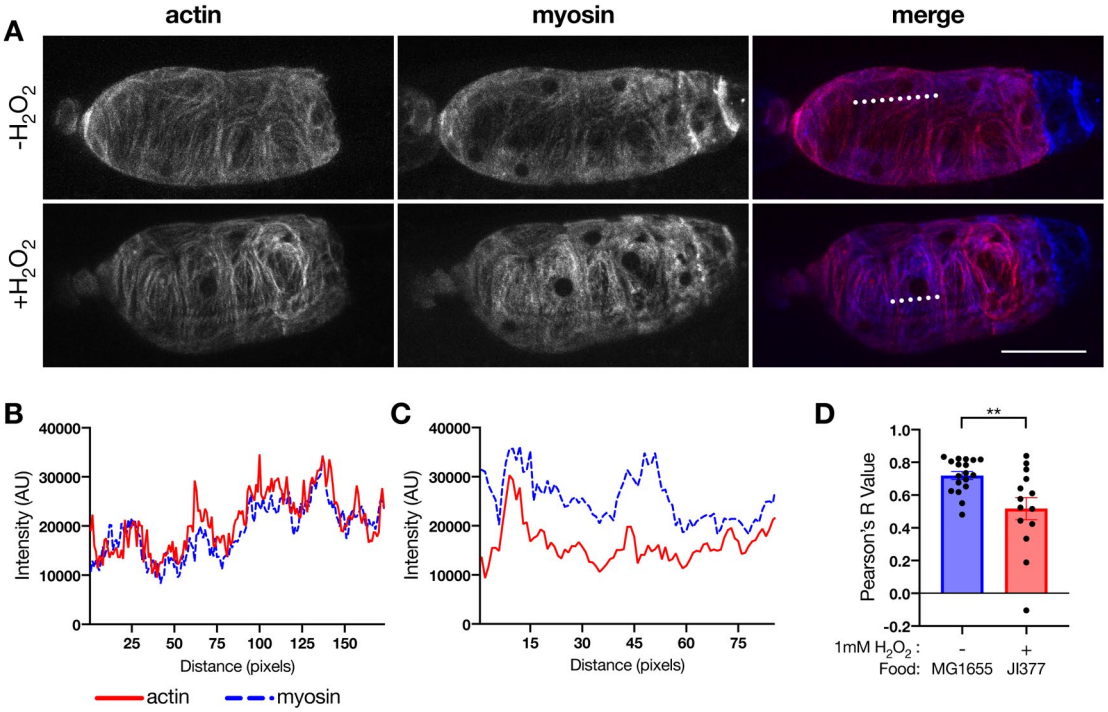

FIGURE 2: Exogenous hydrogen peroxide treatment reduces actomyosin colocalization. (A) Representative confocal maximum-intensity projections of spermathecae labeled with moeABD::mCherry and GFP::NMY-1 and either untreated (NGM+MG1655) or treated (1 mM H_2O_2 +JI377) for 45 min before imaging. Plotted fluorescence intensities across a 10 pixel–wide line (dotted line in A) for either untreated (B) or H_2O_2-treated (C) cells. Pearson's *R* coefficient is plotted for each cell measured. Untreated, $n = 18$ cells (5 animals); 1 mM H_2O_2, $n = 14$ (4 animals). Error bars are SEM. Unpaired *t* test: * $p \leq 0.05$.

previous-generation sensor that has been used in *C. elegans*, roGFP::ORP1, but with increased sensitivity to H_2O_2 oxidation (Gutscher *et al.*, 2009; De Henau *et al.*, 2015; Morgan *et al.*, 2016). We validated the sensitivity and measured the dynamic range of the sensor using excised gonads treated chemically with either oxidizing or reducing agents, or as a control with N-ethylmaleimide (NEM), a compound that blocks free thiols from further oxidation (Hansen and Winther, 2009; Figure 1, H and I). We observed that without treatment with exogenous H_2O_2, an H_2O_2 gradient is observed across the spermatheca, where the more distal cells and the sp-ut valve displayed lower levels of H_2O_2, while the more central and proximal bag cells had higher levels (Figure 1H). Treatment of live animals with 1 mM exogenous H_2O_2 resulted in further oxidation of the sensor within the spermatheca (Figure 1J). Together, these results suggest that endogenous H_2O_2 is not uniformly distributed over the spermatheca and that exogenous H_2O_2 treatment further enhances H_2O_2 levels. Differential H_2O_2 levels could contribute to altered redox signaling through local oxidation of client proteins (Stöcker *et al.*, 2018).

Exogenous addition of H_2O_2 results in the embryo spending less time in the spermatheca. This change could be due to increased contractility in the spermathecal bag, which could force the embryo out prematurely (Tan and Zaidel-Bar, 2015), or, conversely, could be the result of premature opening of a less contractile sp-ut valve (Kelley *et al.*, 2018). If the spermathecal bag cells were more contractile, we would expect to see faster exit times to accompany the shorter dwell times. However, we observed slower exit times with H_2O_2 treatment (see Figure 1D), suggesting both the bag and the valve cells are less contractile. To test the idea that the spermathecal tissue is less contractile when treated with H_2O_2, we observed the actomyosin cytoskeleton in treated and untreated animals. We have shown previously that oocyte entry triggers myosin activation, resulting in organization of the actin network into bundles and an increase in actomyosin colocalization (Wirshing and Cram, 2017; Kelley *et al.*, 2018). We treated animals colabeled with GFP::NMY-1 and the F-actin binding protein moeABD::mCherry on H_2O_2 plates as described above. Treated animals exhibited less colocalization of actin and myosin than untreated animals (Figure 2, A–D). This suggests that H_2O_2 treatment results in reduced myosin activity, consistent with the reduced contractility and the altered transit time of the ovulations observed after H_2O_2 treatment.

Exogenous hydrogen peroxide inhibits Rho activity

RHO-1/Rho and its downstream effector, LET-502/ROCK, drive spermathecal contractility (Wissmann *et al.*, 1999; Tan and Zaidel-Bar, 2015; Kelley *et al.*, 2018). RHO-1/Rho has two conserved cysteines adjacent to the active site in the GTP-binding pocket of the protein (Ihara *et al.*, 1998; Figure 3A). Formation of a disulfide bond between these cysteines blocks GTP binding and inhibits Rho activity (Gerhard *et al.*, 2003; Mitchell *et al.*, 2013; Xu and Chisholm, 2014). To determine if the observed differences in ovulation timing were dependent on the oxidation of RHO-1, we used animals in which the endogenous cysteine 20 had been replaced with alanine (RHO-1(C20A)) using CRISPR, rendering it less sensitive to oxidizing conditions. Unlike wild-type transits, which responded to H_2O_2 treatment, transit parameters and actomyosin colocalization in RHO-1(C20A) animals treated with H_2O_2 exhibited no differences from those in untreated animals (Figure 3, B–D). These data suggest that cysteine oxidation of RHO-1 plays an important role in the response of the spermatheca to oxidizing conditions.

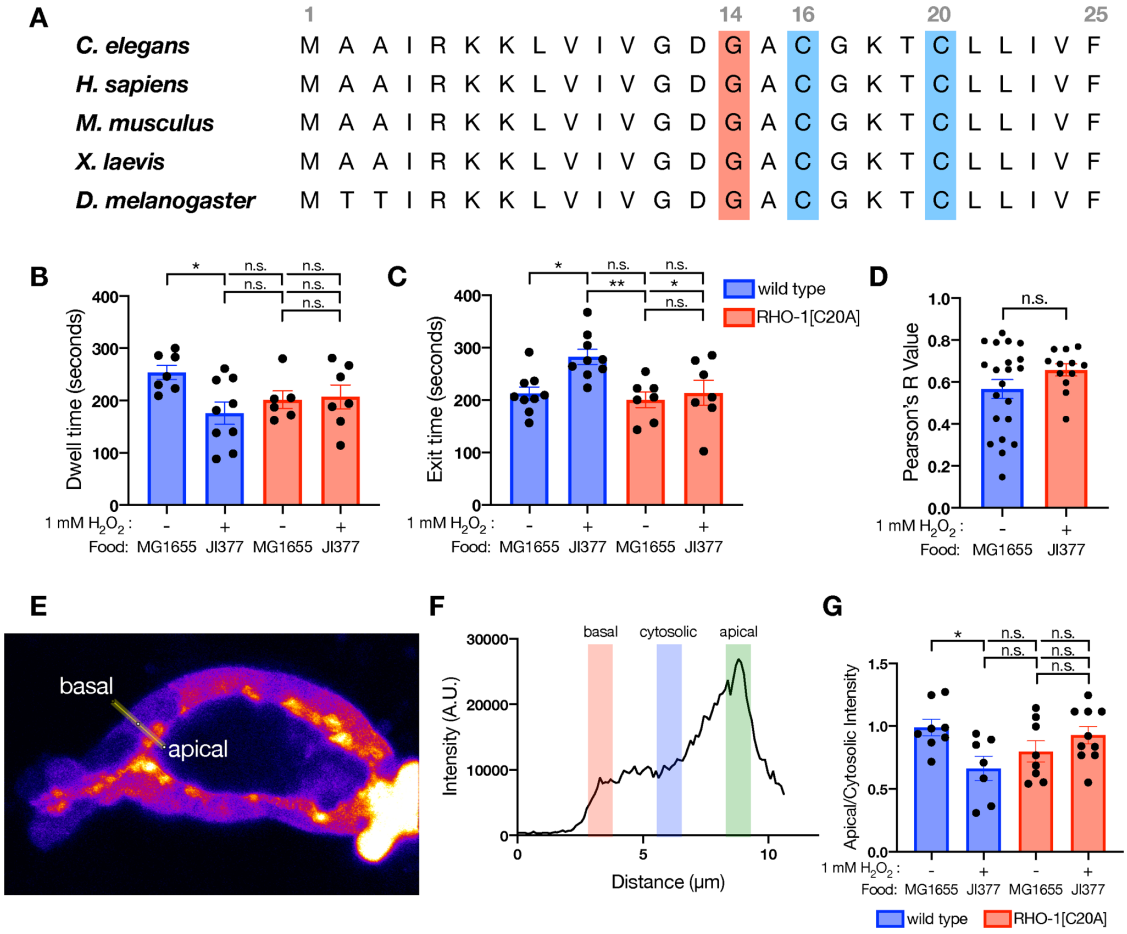

FIGURE 3: RHO-1/Rho is redox-sensitive and hydrogen peroxide treatment reduces its activity. (A) Alignment of residues 1–25 in *C. elegans*, *H. sapiens*, *M. musculus*, *X. laevis*, and *D. melanogaster* Rho shows the conserved active site, G14 (red), and redox-sensitive C20 (blue), with resolving C16 (blue) of RhoA. (B) Dwell time is shorter in wild-type animals treated with H_2O_2 (blue bars). RHO-1(C20A) animals no longer exhibit differences in dwell time with or without H_2O_2 treatment (red bars). (C) H_2O_2 treatment of wild-type animals results in longer exit time than for untreated animals (blue bars), but RHO-1(C20A) animals show no significant difference with H_2O_2 treatment (red bars). Each point represents a time measurement taken from a single first ovulation. Data for wild-type animals treated with 1 mM H_2O_2 or not treated (blue bars) are the same points as in Figure 1, C and D. Error bars are SEM. One-way ANOVA with Tukey's multiple comparisons: ns $p > 0.05$, * $p \leq 0.05$, ** $p \leq 0.01$. (D) Measurements of individual cells expressing moeABD::mCherry and GFP::NMY-1 with the RHO-1(C20A) mutation indicates no difference in actomyosin colocalization with or without exogenous H_2O_2 treatment. Untreated = 21 cells (six animals); 1 mM H_2O_2, $n = 12$ (four animals). Error bars are SEM. Unpaired *t* test: ns $p > 0.05$. (E) Representative single *z*-slice of the AHPH::GFP Rho activity sensor with a 10 pixel–wide line drawn from the basal to the apical surface of the spermatheca, with the average of that line plotted in F. From the fluorescent image, the five most basal and five most apical pixels were annotated, and the five pixels midway between those points are considered the cytosolic intensity. (G). Points represent the apical intensity normalized to the cytosolic intensity. In wild-type animals (blue bars), exogenous H_2O_2 inhibits Rho activity. However, this effect is lost in RHO-1(C20A) animals (red bars). Wild type untreated = eight measurements (four animals); wild type with exogenous H_2O_2 = seven measurements (five animals); C20A untreated = eight measurements (four animals); C20A with exogenous H_2O_2 = 10 measurements (five animals). Error bars are SEM. One-way ANOVA with Tukey's multiple comparisons: ns $p > 0.05$, * $p \leq 0.05$.

To further determine whether RHO-1/Rho activity can be regulated by cysteine oxidation, we used a previously established Rho activity sensor (AHPH::GFP), in which the Rho-binding domain of anillin is fused to GFP (Tse *et al.*, 2012; Tan and Zaidel-Bar, 2015). RHO-1 is predominantly active at the apical membrane, which can be visualized with the Rho activity sensor (Figure 3, E and F; Tan and Zaidel-Bar, 2015). The AHPH::GFP signal at the apical membrane is decreased in H_2O_2–treated animals compared with untreated animals (Figure 3, E–G). In RHO-1(C20A) mutants, no difference in Rho activity in animals treated or not treated with exogenous H_2O_2 was observed (Figure 3G). These data suggest that exogenous H_2O_2 is capable of inhibiting Rho activity in the spermatheca, and that this inhibition is dependent on the oxidation of C20.

SOD-1 regulates the redox environment of the spermatheca

Because we found that the contractility of the spermatheca is sensitive to oxidizing conditions induced by exogenous H_2O_2, we next sought to identify genetic regulators of the spermathecal redox environment under physiological conditions. SOD-1 and SOD-5, the

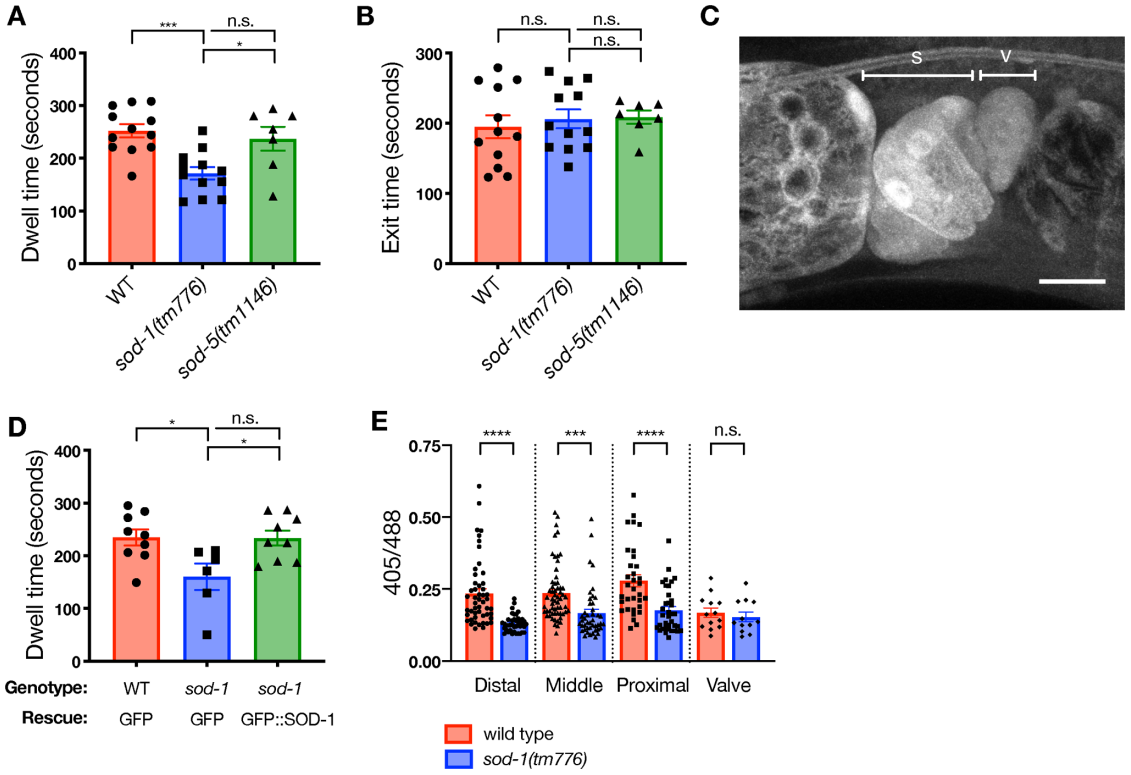

FIGURE 4: SOD-1 regulates hydrogen peroxide–based protein oxidation in the spermathecal bag cells and contractility of the spermatheca. (A) Depletion of *sod-1*, but not *sod-5*, results in shorter dwell times. (B) No significant difference in exit times in *sod-1(tm776)* or *sod-5(tm1146)* animals was observed. Points represent transit measurements from first ovulations. Error bars are SEM. One-way ANOVA with Tukey's multiple comparisons: ns $p > 0.05$, * $p \leq 0.05$, *** $p \leq 0.001$. (C) SOD-1 expression was imaged using a *sod-1p::GFP::sod-1 3′UTR* transcriptional reporter. SOD-1 is expressed in the sheath, the spermathecal bag cells (labeled s), and the sp-ut valve (labeled v). Scale bar is 10 µm. (D) Tissue-specific rescue of GFP::SOD-1 in *sod-1* animals in the spermatheca and sp-ut valve rescues the short transit times seen in *sod-1* animals to wild-type times. Points represent transit measurements from first ovulations. Error bars are SEM. One-way ANOVA with Tukey's multiple comparisons: ns $p > 0.05$, * $p \leq 0.05$. (E) Quantification of protein oxidation measured using the TOMM-20::roGFP::TSA2 redox sensor in live animals. Each point represents an individual mitochondria/mitochondrial cluster measurement from spermathecae that had already had at least one ovulation, but were not occupied during imaging. Loss of *sod-1* results in a more reduced sensor in all regions of the bag, but there is no difference in H_2O_2-based oxidation in the sp-ut valve. Wild type (red bars; $n = 10$ animals) *sod-1(tm776)* (blue bars; $n = 6$ animals). Error bars are SEM. Unpaired *t* test: ns $p > 0.05$, *** $p \leq 0.001$, **** $p \leq 0.0001$.

two cytosolic superoxide dismutases, are responsible for converting superoxide radicals to H_2O_2 in the cytosol (Braeckman *et al.*, 2016). DIC time-lapse microscopy of ovulations revealed that mutation of *sod-1*, but not *sod-5*, resulted in shorter dwell times. Neither resulted in a change in exit time from that in wild type (Figure 4, A and B). Analysis of a transcriptional reporter indicates that *sod-1* is expressed in both the spermatheca and sp-ut valve (Figure 4C). To further explore the role of SOD-1 in spermathecal contractility, we performed a tissue-specific rescue experiment. When SOD-1 was expressed in both the bag and valve using the *fln-1* promoter (Kovacevic and Cram, 2010; DeMaso *et al.*, 2011), we observed complete rescue of the transit defects seen in *sod-1* animals (Figure 4D). This suggests that SOD-1 is required within the spermatheca to regulate contractility.

We next asked whether SOD-1 regulates the redox environment of the spermatheca. To further investigate spatial differences across the spermatheca, we used the genetically encoded tomm-20::roGFP2::TSA2ΔC$_R$ redox sensor (shown in Figure 1H) and digitally sectioned images of each spermatheca from the NEM-treated control by dividing the tissue into thirds plus the sp-ut valve. We then measured individual mitochondrial clusters in each of these regions and found that the distal regions of the spermatheca and sp-ut valve have lower levels of H_2O_2 -sensor oxidation than the central bag cells and that loss of *sod-1* results in lower levels of oxidation of the sensor throughout the spermatheca, with no change in the sp-ut valve (Figure 4F). Taken together, these results suggest that SOD-1 is required in the spermatheca to produce a gradient of H_2O_2 in the bag cells, and that this can be used to mediate redox signaling.

H_2O_2 modulates the activity of RHO-1 through its redox-sensitive cysteine, C20

We next asked whether the shorter dwell times in *sod-1* animals were due to a change in bag or sp-ut valve contractility, and if so, where SOD-1-derived H_2O_2 might be functioning in the spermathecal contractility signaling pathway. The *sod-1* animals have more organized actin in the spermathecal bag than wild-type animals, suggesting an increase in contractility (Figure 5, A and B). To determine whether this effect was mediated through the Rho pathway, we used animals lacking the phospholipase *plc-1*, which have noncontractile spermathecal cells, and as a result, actin bundles remaining poorly aligned (Wirshing and Cram, 2017). We have

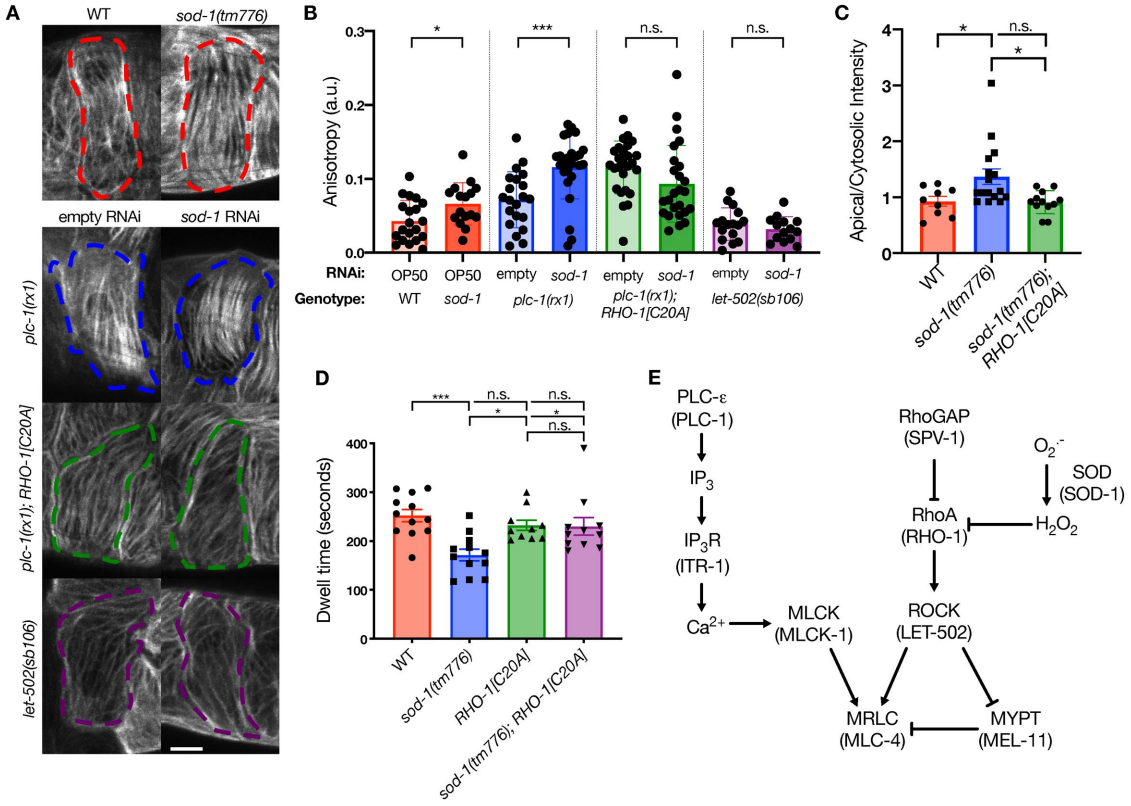

FIGURE 5: SOD-1 increases contractility-dependent actin organization through RHO-1(C20A), independent of calcium signaling and upstream of LET-502/ROCK. (A) Representative cells labeled with ACT-1::GFP. *sod-1(tm776)* animals have more organized actin than wild-type animals on the first ovulation. (B) Loss of *sod-1* can rescue actin organization in *plc-1(rx1)* animals and this rescue is dependent on C20 of RHO-1. However, *sod-1* depletion does not rescue the poor actin organization phenotype in *let-502(sb106)* animals. Points represent anisotropy measured from single cells (examples outlined in A). Error bars are SEM. Unpaired *t* test: ns $p > 0.05$, ** $p \leq 0.01$. (C) *sod-1* animals have increased Rho activity when measured as a ratio of the apical to cytosolic AHPH::GFP intensity but there is no difference between wild type and *sod-1(tm776);rho-1(C20A)* double mutants. WT = nine measurements (five animals); *sod-1(tm776)* = 16 measurements (eight animals); *sod-1(tm776)rho-1(C20A)* = 12 measurements (six animals). Error bars are SEM. Unpaired *t* test: ns $p > 0.05$, * $p \leq 0.05$. (D) The short dwell times seen in *sod-1(tm776)* animals are dependent on C20 of RHO-1. Each point represents a dwell time measured from a first ovulation. Error bars are SEM. One-way ANOVA with Tukey's multiple comparisons: ns $p > 0.05$, * $p \leq 0.05$, *** $p \leq 0.001$. (E) Model for the molecular pathway by which SOD-1 modulates spermathecal contractility, where SOD-1 inhibits contractility by producing H_2O_2, which inhibits RHO-1.

previously shown that increasing activity of the Rho-mediated pathway, which acts in parallel to PLC-1, partially rescues the poor actin fiber alignment of *plc-1* animals (Wirshing and Cram, 2017). We reasoned that if the effect of SOD-1 on spermathecal contractility is mediated through the redox-sensitive inhibition of RHO-1, loss of *sod-1* should also be able to rescue the poor actin alignment of *plc-1* animals through an increase in RHO-1 activity. RNAi of *sod-1* in the *plc-1(rx1)* background significantly rescued alignment and organization of actin compared with controls (Figure 5, A and B). This result suggests that SOD-1 acts in parallel to PLC-1 and likely in the Rho-dependent arm of the pathway. Loss of *sod-1* has no effect on *plc-1(rx1);RHO-1(C20A)* double mutants, suggesting that H_2O_2-dependent oxidation of C20 is required (Figure 5, A and B). To determine where SOD-1 functions in the Rho/ROCK/LET-502 pathway, we fed *let-502(sb106)* animals *sod-1(RNAi)* and saw no rescue of actin organization as compared with controls, suggesting that SOD-1 indeed acts upstream of ROCK/LET-502 in this pathway (Figure 5, A and B).

If RHO-1 activity is decreased when it is oxidized by H_2O_2, then in the absence of *sod-1*, RHO-1 should be more active. To test this hypothesis, we measured Rho activity in *sod-1(tm776)* animals. Loss of *sod-1* resulted in elevated Rho activity at the apical surface comparable to that in wild-type animals, and this elevated Rho activity depended on C20 (Figure 5C). Additionally, we found that the short dwell times seen in *sod-1(tm776)* animals are dependent on C20 of RHO-1 (Figure 5D). This suggests that the effects of *sod-1* on transit times and actin organization depend on the oxidation of C20 and inhibition of RHO-1 (Figure 5E).

DISCUSSION

Contractility in the spermatheca is regulated by Rho and calcium-mediated pathways, which converge on the activation of myosin and are required for the spermathecal bag to contract (Wissmann *et al.*, 1999; Kariya *et al.*, 2004; Kovacevic *et al.*, 2013; Tan and Zaidel-Bar, 2015; Wirshing and Cram, 2017; Kelley *et al.*, 2018). Here, we discovered that contractility in the spermatheca is sensitive to H_2O_2. We observed an H_2O_2 gradient across the spermatheca, with the highest levels found in the central cells of the spermatheca bag. This gradient is dependent on the cytosolic superoxide dismutase SOD-1 and modulates contractility of the spermatheca through inhibition of RHO-1, independently of calcium signaling and upstream of LET-502/ROCK.

Our results suggest that lowering Rho through oxidation and formation of a disulfide bond between C16 and C20 lead to decreased actomyosin fiber formation and decreased contractility in the spermatheca. While several labs have published that Rho is redox- sensitive, different oxidants appear to yield either increases or decreases in activity (Gerhard *et al.*, 2003; Heo *et al.*, 2006; Aghajanian *et al.*, 2009; Xu and Chisholm, 2014; Horn *et al.*, 2017). Direct oxidation of Rho by $1e^-$ oxidants in vitro results in oxidation of C20 and enhanced nucleotide exchange, due to poor nucleotide binding (Heo and Campbell, 2005; Horn *et al.*, 2017). However compounds that promote formation of a disulfide bond between C16 and C20 are expected to result in Rho inhibition (Gerhard *et al.*, 2003; Heo *et al.*, 2006; Xu and Chisholm, 2014). Our results suggest that exogenous application of H_2O_2 decreases Rho-mediated myosin activity through oxidation of RHO-1(C20). This is consistent with in vitro (Gerhard *et al.*, 2003; Heo *et al.*, 2006) and in vivo (Xu and Chisholm, 2014) data demonstrating that ROS can inhibit Rho activity and the observation that exogenous addition of phenylarsine oxide (PAO), a cross-linker of nearby thiol groups, inhibits Rho, but not other Rho family GTPases that lack the resolving cysteine C16 (Gerhard *et al.*, 2003).

We found that the superoxide dismutase SOD-1 is needed to maintain wild-type H_2O_2-dependent redox signaling in the spermathecal bag. Loss of *sod-1* results in less oxidation of the roGFP2::Tsa2 ΔC_R H_2O_2 sensor, consistent with the role of SOD-1 in converting superoxide to H_2O_2 (Fukai and Ushio-Fukai, 2011). Given that wild-type animals have a relatively high level of H_2O_2, which appears to be generated from an original pool of superoxide anions, it would be interesting to identify the source of superoxide in these cells. Some potential sources could be the mitochondrial electron transport chain (Grivennikova and Vinogradov, 2006; Bleier and Dröse, 2013; Wong *et al.*, 2017) and one of the two DUOX *C. elegans* NADPH oxidases (Edens *et al.*, 2001; Meitzler and Ortiz de Montellano, 2009).

We observed no differences in H_2O_2 levels in the sp-ut valve in *sod-1* animals, perhaps because of functional redundancy with another enzyme. Additionally, in wild-type animals, H_2O_2-mediated oxidation of the sensor was lower in the sp-ut valve than in the rest of the spermathecal tissue. We have previously shown that the Rho pathway is particularly important in regulating the timing of embryo transits through the spermatheca via its effects on valve contractility (Kelley *et al.*, 2018). This result suggests that in addition to differences in expression, such as the high expression of LET-502/ROCK in the sp-ut valve (Wissmann *et al.*, 1999; Kelley *et al.*, 2018), the reduced valve may provide a permissive environment for increased Rho activity, while the more oxidizing regions decrease Rho activity.

Human cytosolic superoxide dismutase, SOD1, is one of the most commonly mutated proteins in ALS patients, with more than 100 disease-associated alleles in patients (Rosen *et al.*, 1993; Saccon *et al.*, 2013; Pansarasa *et al.*, 2018). Mutations result in altered SOD1 activity, the formation of insoluble toxic aggregates, and subsequent loss of motor neuron function (Cuanalo-Contreras *et al.*, 2013; Saccon *et al.*, 2013; Pansarasa *et al.*, 2018). In addition to motor neuron disfunction, other manifestations of the disease include altered blood pressure (Cuanalo-Contreras *et al.*, 2013) and hypertension (Lee and Lee, 2012). Several protein kinases control vasoconstriction and blood pressure through redox signaling (Ray *et al.*, 2011; Burgoyne *et al.*, 2013). This work offers new insights into other potential redox-regulated targets that can affect the contractility of vasculature in patients with SOD1 mutations. The *C. elegans* spermatheca may offer a useful tool for studying SOD-1 effects on the contractility of biological tubes to model disease states.

MATERIALS AND METHODS

Strain generation and maintenance of nematodes

Unless otherwise noted, all strains were grown at 23°C on Nematode growth medium (NGM; 0.107 M NaCl, 0.25% wt/vol peptone, 1.7% wt/vol BD Bacto-Agar, 2.5 mM KPO_4, 0.5% Nyastatin, 0.1 mM $CaCl_2$, 0.1 mM $MgSO_4$, 0.5% wt/vol cholesterol) seeded with OP50 *E. coli* (Hope, 1999). Extrachromosomal arrays were injected with constructs between 5 and 20 ng/µl with *rol-6(su1006)* as a coinjection marker as previously reported (Mello *et al.*, 1991). UN1513 was made by UV integrating strain RZB171 msnEx171[sth-1p::AHPH::GFP; pRF4(*rol-6(su1006)*)] (Tan and Zaidel-Bar, 2015) and then outcrossing the strain three times with N2. UN1757 was generating by crossing HR863 *let-502(sb106)* (Piekny *et al.*, 2000) with UN1502 xbIs1502[ACT-1::GFP; pRF4(*rol-6(su1006)*)] (Wirshing and Cram, 2017).

See Supplemental Table 1 for a complete list of strains.

RNAi treatment

RNAi feeding was performed as described previously (Kovacevic and Cram, 2010): HT115(DE3) bacteria containing a double-stranded RNA construct in the T444T backbone (Sturm *et al.*, 2018) were grown in Luria broth (LB) overnight at 37°C in a shaking incubator. Bacteria were seeded onto NGM plates supplemented with 25 µg/ml carbenicillin and 1 mM isopropylthio-β-galactoside (IPTG).

Molecular cloning

pUN615 fln-1p::GFP::sod-1::fln-1 3′utr. pUN615 was generated by amplifying the *sod-1* gene from genomic DNA (gDNA) with primers (F 5′ aaaacccgggatgtttatgaatcttctcactc 3′; R 5′ AAAAGGTACCtgatataatgagcagagacat 3′) that added the restriction sites *XmaI* and *KpnI* to the 5′ and 3′ ends of the amplicon, respectively. The PCR product was digested and cloned into pUN236 (*fln-1p::GFP::inx-12::fln-1 3′utr*) in place of the *inx-12* gene.

pUN839 fln-1p::tomm-20::roGFP2::TSA2ΔC$_R$::fln-1 3′utr. The tomm-20::roGFP2:: TSA2ΔC_R sequence was amplified from the *fbf-1p*::tomm-20::roGFP2::TSA2ΔC_R::tbb-2 3′ UTR with primers (F 5′ aaaaTCTAGAATGTCGGACACAATTCTTGGT 3′; R 5′ aaaaGGTACCTTAGTTGTTAGCGTTCTTGAAGTA 3′) that added *XbaI* and *KpnI* restriction sites to the 5′ and 3′ ends, respectively. The PCR product was cloned using restriction cloning into pUN85 (*fln-1p::fln-1 3′UTR*).

pUN1216 sod-1 in T444T. The *sod-1* sequence used in the Vidal library was cloned into the T444T vector using NEB Builder. The sequence was initially amplified with the following primers that anneal outside the gene-specific sequence: F 5′ ctatagggagaccggcagatctgattaatacgactcactataggg 3′; R 5′ GGTCGACGGTATCACTCACTATAGGG 3′. This sequence was then cloned into the *EcoRV* site of T444T using NEB Builder.

pUN1241 sod-1p::GFP::sod-1 3′UTR. The *sod-1* promoter and 3′ UTR were amplified off of gDNA using the following primers: Promoter: F 5′ TCACAACGATGGATACGCTAACAACatataccaaactgatcggaca 3′, R 5′ CTTTACTCATTTTTTCTACCGGTACcaccgatctaaaatactga 3′; UTR: F 5′ GAACTATACAAATAGCATTCGTAGActacctgaatcgcgtctctg 3′, R TCTGCTCTGATGCCGCATAGTTAAGaatcgcccttctccgtcag 3′. GFP and the backbone of pUN71 (*fln-1p::GFP::fln-1 3′UTR in pPD95_77*) were amplified using the following primers: GFP: F 5′ GTACCGGTAGAAAAAATG 3′, R 5′ TCTACGAATGCTATTTGTA 3′; backbone: F 5′ CTTAACTATGCGGCATCAG 3′, R 5′ GTTGTTAGCGTATCCATCGT 3′. Fragments were purified and assembled using NEB Builder.

Generation of endogenous RHO-1(C20A)

The RHO-1(C20A) strain was generated using a co-CRISPR approach (Ward, 2015). An injection mix containing plasmid pJW1285 that drives expression of Cas9 and *pha-1(e2123)* sgRNA (60 ng/µl, Addgene #61252), the *pha-1(e2123)* PAGE-purified 80mer single-stranded oligodeoxynucleotide (ssODN) HR template (50 ng/µl), two plasmids expressing sgRNAs targeting the *rho-1* locus (50 ng/µl each), and a 100mer ssODN HR template to introduce the desired mutations in *rho-1* (100 ng/µl) was injected into the germline of young adult *pha-1(e2123)* worms (strain GE24). sgRNA plasmids targeting the *rho-1* locus were generated by ligation of annealed oligo pairs into BbsI-digested pJJR50 (Addgene #75026). Sequences of the oligonucleotides used for the generation of *rho-1* mutants can be found in Supplemental Table S2. Injected animals were placed at 25°C and offspring with edited *rho-1* alleles were identified by singling out surviving F1 progeny of injected animals, allowing them to lay eggs followed by lysis with 20 µg/mL Proteinase K. Lysates were used as input in PCR reactions using a *rho-1* F/R primer pair and point mutations were confirmed by Sanger sequencing of the *rho-1* amplicon. This strain (TBD273) was then outcrossed three times with the wild type to generate UN1785, used in all experiments.

Sequence alignment

Sequences for first 25 amino acids of RhoA or the closest ortholog of the species shown were identified from Uniprot (Consortium TU, 2010) and aligned using ClustalOmega (Sievers *et al.*, 2011; McWilliam *et al.*, 2013; Li *et al.*, 2015). Uniprot entry IDs are as follows: *C. elegans* (Q22038), *Homo sapiens* (P61586), *Mus musculus* (Q9QUI0), *Xenopus laevis* (Q9W760), *Drosophila melanogaster* (P48148).

Exogenous hydrogen peroxide treatment

To treat animals with exogenous H_2O_2, we supplemented NGM plates with 1 mM H_2O_2. Plates were allowed to dry for 1 day and then seeded with either MG1655 (wild type) or JI377 (ΔahpCF katG katE; Seaver and Imlay, 2001) *E. coli*. Food was allowed to dry for at least 24 h before use, and plates were always made fresh (<5 d) before use. Acute treatment of animals was achieved by transferring adult worms, which had not ovulated yet, to either NGM or 1 mM H_2O_2 NGM plates seeded with either MG1655 or JI377 for 45 min at 23°C. Animals were immediately imaged (described below) for ≤1 h.

Exogenous *tert*-butyl hydroperoxide treatment

We supplemented NGM plates with 1 mM tert-butyl hydroperoxide. Plates were allowed to dry for 1 day and then seeded with OP50 *E. coli*. Food was dried for at least 1 day, and was always made fresh (<5 d) before use. Animals were grown on plain NGM with OP50 to adulthood and then transferred to the 1 mM tert-butyl plates for 45 min before imaging. Animals were then immediately transferred to a slide and imaged for ≤1 h.

DIC time-lapse imaging

Animals were synchronized using an "egg prep" procedure. Gravid hermaphrodites were lysed using an alkaline hypochlorite solution, and then the embryos were washed in M9 buffer (22 mM KH_2PO_4, 42 mM $NaHPO_4$, 86 mM NaCl, and 1 mM $MgSO_4$; Hope, 1999). Animals were grown at 23°C for ~50–54 h. Adults were immobilized on a 5% agarose slide with a 1:1:1.5 ratio of water, M9 buffer, and 0.05-µm Polybead microspheres (Polysciences). First ovulations were imaged using a Nikon Eclipse 80i microscope with a 60× oil-immersion lens, a charge-coupled device camera, and SPOT R3 software. Ovulations were imaged at a rate of 1 Hz and analyzed using ImageJ.

Excising, treating, and fixing redox-sensor gonads

We adapted the protocol below from one originally described for *D. melanogaster* (Albrecht *et al.*, 2011). UN1846 worms were enriched for the redox sensor by putting gravid rollers into 10% sodium hypochlorite in M9 Buffer solution on a fresh NGM plate seeded with OP50. Offspring hatched, and after ~60 h at 23°C gonads were excised using watch glasses and 23-gauge needles and incubated in one of the following solutions for 10 min at room temperature: 20 mM NEM, 2 mM diamide (DA), or 2 or 20 mM hydrogen peroxide (H_2O_2). To fully reduce the sensor, gonads treated with NEM were next treated with 100 mM dithiothreitol (DTT). As a control to ensure that our NEM treatment was sufficiently blocking thiol oxidation, some gonads incubated with NEM were subsequently incubated with 2 mM DA. All solutions were made in phosphate-buffered saline (PBS) at pH 7.0. Animals were rinsed in PBS and then fixed in a 1.6% formaldehyde solution for 25 min at room temperature. Gonads were rinsed twice in PBS and then mounted on a 2% agarose pad on a glass slide, and the coverslip was sealed.

Hydrogen peroxide treatment of live redox sensor–expressing worms

To determine if H_2O_2 treatment resulted in oxidation of proteins within the spermatheca we grew animals on plain NGM plates seeded with JI377 for ~60 h at 23°C. Animals were washed in M9 buffer and then transferred to a slide with a 1.5 × 5–cm 2% agarose pad with either 0 mM H_2O_2 (1:1:1.5 ratio of 0.01% tetramisole and 0.1% tricaine solution in M9 buffer, M9 buffer, and 0.05 µm Polybead microspheres) or 1 mM H_2O_2 (1:1:1.5 ratio of 0.01% tetramisole and 0.1% tricaine solution in M9 buffer, 3.5 mM H_2O_2 in M9 buffer, and 0.05 µm Polybead microspheres). Samples were sealed with a coverslip and imaged immediately.

Confocal imaging

Animals were synchronized using egg prep and imaged as young adults, where only first ovulations were captured. Adults were immobilized on a 5% agarose slide with a 1:1:1.5 ratio of 0.01% tetramisole and 0.1% tricaine solution in M9 buffer, M9 buffer, and 0.05 µm Polybead microspheres. Images were captured using an LSM 710 confocal microscope (Zeiss) with Zen software (Zeiss) and a Plan-Apochromat 63×/1.49 oil DIC M27 objective or 100×/1.4 oil DIC objective. GFP was imaged using a 488-nm laser, and mCherry was imaged using a 561-nm laser. For actomyosin imaging, time-lapse *z*-stacks of 20 slices were captured at 12-s intervals using the 63× objective similarly to the approach described previously (Wirshing and Cram, 2017). For the AHPH Rho activity sensor, a single 2.1-µm slice was imaged over time to capture a thin sagittal section of the spermatheca at a rate of 1 Hz with the 63× objective. The roGFP2::Tsa2 redox sensor was imaged using sequential excitation of 405- and 488-nm lasers with emission detection at 499–601 nm on the 100× objective. Fixed and live worms were imaged at 0.39-µm intervals. Fixed samples had each slice averaged two times. To image actin alignment, we used methods described previously (Wirshing and Cram, 2017). For *plc-1* worms, images were taken on spermathecae occupied by single-celled embryos with 0.38-µm intervals and averaged two times. For all other genotypes, movies were captured with 40 slices at 15-s intervals.

Image analysis

All image analysis was done using ImageJ software. For analysis of actin and myosin colocalization, a maximum intensity projection from the frame where the sp-ut valve began to open was used. A 10 pixel–wide line was drawn across individual cells from the central

bag region of the spermatheca. For colocalization analysis, intensities across each line were put into GraphPad Prism software and used to measure the Pearson's *R* value of each cell. Rho activity was measured using the single sagittal slice of the frame where the sp-ut valve began to open. A line 10 pixels wide was drawn from the basal to the apical side in the distal region of the spermatheca. The apical/cytosolic intensity plotted is the average of the five most apical pixels divided by the average of five cytosolic pixels. The cytosolic region was determined by finding the midpoint between the most basal and most apical pixels. To quantify the redox sensor in live animals treated with either 0 or 1 mM H_2O_2, we used the sum-intensity projections of the image stacks. Spermathecae were outlined using the polygon selection tool in ImageJ; then the average intensity for the 488 and 405 channels was quantified for each ROI. Only animals that had their spermathecae occupied with an embryo were quantified. To measure the redox sensor in chemically treated excised gonads, the background was first subtracted using the rolling-ball procedure (50 pixels), and then sum-intensity projections were made of the stacks. We measured the average intensity across the entire image in both the 405 and 488 excitation intensities and divided the 405/488 values to plot. To analyze spatial differences in redox sensor measurements, we also subtracted the background using the rolling-ball procedure (50 pixels) and then made a sum-intensity projection of the stacks. Individual mitochondria or mitochondrial clusters were outlined using the freehand tool of ImageJ. Next we measured the mean intensity for that area in both the 405 and 488 channels and plotted the 405/488 values (Gutscher *et al.*, 2009; Albrecht *et al.*, 2011). To determine what region of the spermatheca each measurement fell into, the length of each spermatheca was measured and divided into distal, middle, and proximal thirds or annotated as being in the sp-ut valve. For visualization of the sensor (Figure 5Ei), both channels were initially filtered using a Gaussian blur, the 488 channel was then thresholded, and the 405 image was divided by the 488 image. Actin organization was quantified as previously published using the ImageJ macro FibrilTool (Boudaoud *et al.*, 2014; Wirshing and Cram, 2017). Individual cells were outlined and anisotropy measured using maximum-intensity projections of the images. For movies, the frame where the sp-ut valve began to open is the frame that was measured.

Statistical analysis

We used GraphPad Prism software for all statistical analysis performed. To compare two groups, an unpaired *t* test was used, assuming the data had a normal distribution. To compare three or more groups, ordinary one-way analysis of variance (ANOVA) was performed with a Tukey's multiple comparison test to compare the mean of each group with that of every other group. In all graphs, symbols are represented as follows: $p > 0.05$, * $p \leq 0.05$, ** $p \leq 0.01$, *** $p \leq 0.001$, **** $p \leq 0.0001$

ACKNOWLEDGMENTS

We thank Safuwra Wizzard, who was funded through NSF REU Site Award (1757443), for technical assistance, and Javier Apfeld and members of the Cram and Apfeld labs for helpful feedback and discussions. This work was supported by a National Science Foundation award (1816640) to E.J.C., NWO grant 016.Veni.181.051 to S.D.H., and a grant from the Dutch Cancer Society KWF UU 2014-6902 to T.B.D. Some *C. elegans* strains were provided by the *Caenorhabditis* Genetics Center, which is funded by the National Institutes of Health Office of Research Infrastructure Programs (P40 OD010440).

REFERENCES

Aghajanian A, Wittchen ES, Campbell SL, Burridge K (2009). Direct activation of RhoA by reactive oxygen species requires a redox-sensitive motif. PLoS One 4, 1–10.

Albrecht SC, Barata AG, Großhans J, Teleman AA, Dick TP (2011). In vivo mapping of hydrogen peroxide and oxidized glutathione reveals chemical and regional specificity of redox homeostasis. Cell Metab 14, 819–829.

Amano M, Chihara K, Kimura K, Fukata Y, Nakamura N, Matsuura Y, Kaibuchi K (1997). Formation of actin stress fibers and focal adhesions enhanced by Rho-kinase. Science (80-.) 275, 1308–1311.

An JH, Vranas K, Lucke M, Inoue H, Hisamoto N, Matsumoto K, Blackwell TK (2005). Regulation of the *Caenorhabditis elegans* oxidative stress defense protein SKN-1 by glycogen synthase kinase-3. Proc Natl Acad Sci 102, 16275–16280.

Beach JR, Brynn KS, Shao L, Li D, Swider Z, Remmert K, Zhang Y, Conti MA, Adelstein RS, Rusan NM, *et al.* (2017). Actin dynamics and competition for myosin monomer govern the sequential amplification of myosin filaments. Nat Cell Biol 19, 85–93.

Bedard K, Lardy B, Krause K (2007). NOX family NADPH oxidases: not just in mammals. Biochimie 89, 1107–1112.

Birben E, Sahiner UM, Sackesen C, Erzurum S, Kalayci O (2012). Oxidative stress and antioxidant defense. World Allergy Organ J 5, 9–19.

Biswas S, Chida AS, Rahman I (2006). Redox modifications of protein—thiols: emerging roles in cell signaling. Biochem Pharmacol 71, 551–564.

Bleier L, Dröse S (2013). Superoxide generation by complex III: from mechanistic rationales to functional consequences. Biochim Biophys Acta Bioenerg 1827, 1320–1331.

Boudaoud A, Burian A, Borowska-Wykret, Uyttewaal M, Wrzalik R, Kwiatkowska D, Hamant O (2014). FibrilTool, an ImageJ plug-in to quantify fibrillar structures in raw microscopy images. Nat Protoc 9, 457–463.

Bouffard J, Cecchetelli AD, Clifford C, Sethi K, Zaidel-Bar R, Cram EJ (2019). The RhoGAP SPV-1 regulates calcium signaling to control the contractility of the *C. elegans* spermatheca during embryo transits. Mol Biol Cell.

Braeckman BP, Smolders A, Back P, De Henau S (2016). In vivo detection of reactive oxygen species and redox status in *Caenorhabditis elegans*. Antioxid Redox Signal 25, 577–592.

Bui YK, Sternberg PW (2002). *Caenorhabditis elegans* inositol 5-phosphatase homolog negatively regulates inositol 1,4,5- triphosphate signaling in ovulation. Mol Biol Cell 13, 1641–1651.

Burgoyne JR, Oka S-I, Ale-Agha N, Eaton P (2013). Hydrogen peroxide sensing and signaling by protein kinases in the cardiovascular system. Antioxid Redox Signal 18, 1042–1052.

Citalán-Madrid AF, Vargas-Robles H, García-Ponce A, Shibayama M, Betanzos A, Nava P, Salinas-Lara C, Rottner K, Mennigen R, Schnoor M (2017). Cortactin deficiency causes increased RhoA/ROCK1-dependent actomyosin contractility, intestinal epithelial barrier dysfunction, and disproportionately severe DSS-induced colitis. Mucosal Immunol 10, 1237–1247.

Clempus RE, Griendling KK (2006). Reactive oxygen species signaling in vascular smooth muscle. Cardiovasc Res 71, 216–225.

Consortium TU (2010). The Universal Protein Resource (UniProt) in 2010. Nucleic Acids Res 38, D142–D148.

Conti MA, Adelstein RS (2008). Nonmuscle myosin II moves in new directions. J Cell Sci 121, 404–404.

Cuanalo-Contreras K, Mukherjee A, Soto C (2013). Role of protein misfolding and proteostasis deficiency in protein misfolding diseases and aging. Int J Cell Biol 2013, 1–10.

De Henau S, Tilleman L, Vangheel M, Luyckx E, Trashin S, Pauwels M, Germani F, Vlaeminck C, Vanfleteren JR, Bert W, *et al.* (2015). A redox signalling globin is essential for reproduction in *Caenorhabditis elegans*. Nat Commun 6, 8782.

DeMaso CR, Kovacevic I, Uzun A, Cram EJ (2011). Structural and functional evaluation of *C. elegans* filamins FLN-1 and FLN-2. PLoS One 6, e22428.

Dickinson BC, Chang CJ (2011). Chemistry and biology of reactive oxygen species in signaling or stress responses. Nat Chem Biol 7, 504–511.

Doeing DC, Solway J (2013). Airway smooth muscle in the pathophysiology and treatment of asthma. J Appl Physiol 114, 834–843.

Doonan R, McElwee JJ, Matthijssens F, Walker GA, Houthoofd K, Back P, Matscheski A, Vanfleteren JR, Gems D (2008). Against the oxidative damage theory of aging: superoxide dismutases protect against oxidative stress but have little or no effect on life span in *Caenorhabditis elegans*. Genes Dev 22, 3236–3241.

Edens WA, Sharling L, Cheng G, Shapira R, Kinkade JM, Lee T, Edens HA, Tang X, Sullards C, Flaherty DB, *et al.* (2001). Tyrosine cross-linking of extracellular matrix is catalyzed by Duox, a multidomain oxidase/peroxidase with homology to the phagocyte oxidase subunit gp91 phox. J Cell Biol 154, 879–892.

Finkel T (2011). Signal transduction by reactive oxygen species. J Cell Biol 194, 7–15.
Fukai T, Ushio-Fukai M (2011). Superoxide dismutases: role in redox signaling, vascular function, and diseases. Antioxid Redox Signal 15, 1583–1606.
Gally C, Wissler F, Zahreddine H, Quintin S, Landmann F, Labouesse M (2009). Myosin II regulation during *C. elegans* embryonic elongation: LET-502/ROCK, MRCK-1 and PAK-1, three kinases with different roles. Development 136, 3109–3119.
Gerhard R, John H, Aktories K, Just I (2003). Thiol-modifying phenylarsine oxide inhibits guanine nucleotide binding of Rho but not of Rac GTPases. Mol Pharmacol 63, 1349–1355.
Gissendanner CR, Kelley K, Nguyen TQ, Hoener MC, Sluder AE, Maina CV (2008). The *Caenorhabditis elegans* NR4A nuclear receptor is required for spermatheca morphogenesis. Dev Biol 313, 767–786.
Grivennikova VG, Vinogradov AD (2006). Generation of superoxide by the mitochondrial Complex I. Biochim Biophys Acta Bioenerg 1757, 553–561.
Gunst SJ, Tang DD, Opazo Saez A (2003). Cytoskeletal remodeling of the airway smooth muscle cell: a mechanism for adaptation to mechanical forces in the lung. Respir Physiol Neurobiol 137, 151–168.
Gutscher M, Sobotta MC, Wabnitz GH, Ballikaya S, Meyer AJ, Samstag Y, Dick TP (2009). Proximity-based protein thiol oxidation by H2O2-scavenging peroxidases. J Biol Chem 284, 31532–31540.
Hansen RE, Winther JR (2009). An introduction to methods for analyzing thiols and disulfides: reactions, reagents, and practical considerations. Anal Biochem 394, 147–158.
Hartl L, Huelsz-Prince G, van Zon J, Tans SJ (2019). Apical constriction is necessary for crypt formation in small intestinal organoids. Dev Biol 450, 76–81.
Heo J, Campbell SL (2005). Mechanism of redox-mediated guanine nucleotide exchange on redox-active Rho GTPases. J Biol Chem 280, 31003–31010.
Heo J, Raines KW, Mocanu V, Campbell SL (2006). Redox regulation of RhoA. Biochemistry 45, 14481–14489.
Hope IA (1999). C. elegans: A Practical Approach, Oxford: Oxford University Press.
Horn A, Van Der Meulen JH, Defour A, Hogarth M, Sreetama SC, Reed A, Scheffer L, Chandel NS, Jaiswal JK (2017). Mitochondrial redox signaling enables repair of injured skeletal muscle cells. Sci Signal 10, 1–12.
Hubbard EJA, Greenstein D (2000). The *Caenorhabditis elegans* gonad: a test tube for cell and developmental biology. Dev Dyn 218, 2–22.
Ihara K, Muraguchi S, Kato M, Shimizu T, Shirakawa M, Kuroda S, Kaibuchi K, Hakoshima T (1998). Crystal structure of human RhoA in a dominantly active form complexed with a GTP analogue. J Biol Chem 273, 9656–9666.
Kariya KI, Kim Bui Y, Gao X, Sternberg PW, Kataoka T (2004). Phospholipase C epsilon regulate ovulation in *Caenorhabditis elegans*. Dev Biol 274, 201–210.
Kelley C, Cram E (2019). *Regulation ofactin dynamicsin the* C. elegans somatic gonad. J Dev Biol 7, 6.
Kelley CA, Wirshing ACE, Zaidel-Bar R, Cram EJ (2018). The myosin light-chain kinase MLCK-1 relocalizes during *Caenorhabditis elegans* ovulation to promote actomyosin bundle assembly and drive contraction. Mol Biol Cell 29, 1975–1991.
Kimura K, Ito M, Amano M, Chihara K, Fukata Y, Nakafuku M, Yamamori B, Feng J, Nakano T, Okawa K, *et al*. (1996). Regulation of myosin phosphatase by Rho and Rho-associated kinase (Rho-kinase). Science (80-.) 273, 245–248.
Kovacevic I, Cram EJ (2010). FLN-1/Filamin is required for maintenance of actin and exit of fertilized oocytes from the spermatheca in *C. elegans*. Dev Biol 347, 247–257.
Kovacevic I, Orozco JM, Cram EJ (2013). Filamin and phospholipase C-ε are required for calcium signaling in the *Caenorhabditis elegans* spermatheca. PLoS Genet 9, e1003510.
Lee HL, Lee JK (2012). Amyotrophic lateral sclerosis with an acute hypertensive crises. Ann Rehabil Med 36, 418.
Li W, Cowley A, Uludag M, Gur T, Mcwilliam H, Squizzato S, Park YM, Buso N, Lopez R (2015). The EMBL-EBI bioinformatics web and programmatic tools framework. Nucleic Acids Res 43, W580–W584.
Lints R, Hall DH (2009). Reproductive system, somatic gonad. In: WormAtlas.
Maruyama R, Velarde NV, Klancer R, Gordon S, Kadandale P, Parry JM, Hang JS, Rubin J, Stewart-Michaelis A, Schweinsberg P, *et al*. (2007). EGG-3 Regulates cell-surface and cortex rearrangements during egg activation in *Caenorhabditis elegans*. Curr Biol 17, 1555–1560.
Mason FM, Tworoger M, Martin AC (2013). Apical domain polarization localizes actin-myosin activity to drive ratchet-like apical constriction. Nat Cell Biol 15, 926–936.
McCarter J, Bartlett B, Dang T, Schedl T (1997). Soma–germ cell interactions in *Caenorhabditis elegans*: multiple events of hermaphrodite germline development require the somatic sheath and spermathecal lineages. Dev Biol 181, 121–143.
McCarter J, Bartlett B, Dang T, Schedl T (1999). On the control of oocyte meiotic maturation and ovulation in *Caenorhabditis elegans*. Dev Biol 205, 111–128.
McWilliam H, Li W, Uludag M, Squizzato S, Park YM, Buso N, Cowley AP, Lopez R (2013). Analysis tool Web services from the EMBL-EBI. Nucleic Acids Res 41, W597–W600.
Meitzler JL, Ortiz de Montellano PR (2009). *Caenorhabditis elegans* and human dual oxidase 1 (DUOX1) "peroxidase" domains. J Biol Chem 284, 18634–18643.
Mello CC, Kramer JM, Stinchcomb D, Ambros V (1991). Efficient gene transfer in *C. elegans*: extrachromosomal maintenance and integration of transforming sequences. EMBO J 10, 3959–3970.
Mitchell L, Hobbs GA, Aghajanian A, Campbell SL (2013). Redox regulation of Ras and Rho GTPases: mechanism and function. Antioxid Redox Signal 18, 250–258.
Morgan B, Van Laer K, Owusu TNE, Ezerina D, Pastor-Flores D, Amponsah PS, Tursch A, Dick TP (2016). Real-time monitoring of basal H2O2 levels with peroxiredoxin-based probes. Nat Chem Biol 12, 437–443.
Norman KR, Fazzio RT, Mellem JE, Espelt MV, Strange K, Beckerle MC, Maricq AV (2005). The Rho/Rac-family guanine nucleotide exchange factor VAV-1 regulates rhythmic behaviors in *C. elegans*. Cell 123, 119–132.
Pansarasa O, Bordoni M, Diamanti L, Sproviero D, Gagliardi S, Cereda C (2018). SOD1 in amyotrophic lateral sclerosis: "ambivalent" behavior connected to the disease. Int J Mol Sci 19, 1345.
Pedrosa Nunes K, Rigsby CS, Clinton Webb R (2010). RhoA/Rho-kinase and vascular diseases: what is the link? Cell Mol Life Sci 67, 3823–3836.
Piekny AJ, Wissmann A, Mains PE (2000). Embryonic morphogenesis in *Caenorhabditis elegans* integrates the activity of LET-502 Rho-binding kinase, MEL-11 myosin phosphatase, DAF-2 insulin receptor and FEM-2 PP2c phosphatase. Genetics 156, 1671–1689.
Pilipiuk J, Lefebvre C, Wiesenfahrt T, Legouis R, Bossinger O (2009). Increased IP 3 /Ca 2+ signaling compensates depletion of LET-413/DLG-1 in *C. elegans* epithelial junction assembly. Dev Biol 327, 34–47.
Ray R, Murdoch CE, Wang M, Santos CX, Zhang M, Alom-Ruiz S, Anilkumar N, Ouattara A, Cave AC, Walker SJ, *et al*. (2011). Endothelial Nox4 NADPH oxidase enhances vasodilatation and reduces blood pressure in vivo. Arterioscler Thromb Vasc Biol 31, 1368–1376.
Rosen DR, Siddique T, Patterson D, Figlewicz DA, Sapp P, Hentati A, Donaldson D, Goto J, O'Regan JP, Deng HX, *et al*. (1993). Mutations in Cu/Zn superoxide dismutase gene are associated with familial amyotrophic lateral sclerosis. Nature 362, 59–62.
Saccon RA, Bunton-Stasyshyn RKA, Fisher EMC, Fratta P (2013). Is SOD1 loss of function involved in amyotrophic lateral sclerosis? Brain 136, 2342–2358.
San Martin A, Griendling KK (2010). Redox control of vascular smooth muscle migration. Antioxid Redox Signal 12, 625–640.
Schieber M, Chandel NS (2014). ROS function in redox signaling and oxidative stress. Curr Biol 24, R453–R462.
Seaver LC, Imlay JA (2001). Alkyl hydroperoxide reductase is the primary scavenger of endogenous hydrogen peroxide in Escherichia coli. J Bacteriol 183, 7173–7181.
Sellers JR (1981). Phosphorylation-dependent regulation of Limulus myosin. J Biol Chem 256, 9274–9278.
Siedlik MJ, Nelson CM (2015). Regulation of tissue morphodynamics: an important role for actomyosin contractility. Curr Opin Genet Dev 32, 80–85.
Sievers F, Wilm A, Dineen D, Gibson TJ, Karplus K, Li W, Lopez R, McWilliam H, Remmert M, Soding J, *et al*. (2011). Fast, scalable generation of high-quality protein multiple sequence alignments using Clustal Omega. Mol Syst Biol 7, 1–6.
Smiesko V, Johnson P (1993). The Arterial lumen is controlled by flow-related shear stress. Physiology 8, 34–38.
Smith PG, Roy C, Zhang YN, Chauduri S (2003). Mechanical stress increases RhoA activation in airway smooth muscle cells. Am J Respir Cell Mol Biol 28, 436–442.
Stöcker S, Van Laer K, Mijuskovic A, Dick TP (2018). The conundrum of hydrogen peroxide signaling and the emerging role of peroxiredoxins as redox relay hubs. Antioxid Redox Signal 28, 558–573.

Strome S (1986). Fluorescence visualization of the distribution of microfilaments in gonads and early embryos of the nematode *Caenorhabditis elegans*. J Cell Biol 103, 2241–2252.
Sturm Á, Saskő É, Tibor K, Weinhardt N, Vellai T (2018). Highly efficient RNAi and Cas9-based auto-cloning systems for *C. elegans* research. Nucleic Acids Res 46, e105–e105.
Tan PY, Zaidel-Bar R (2015). Transient membrane localization of SPV-1 drives cyclical actomyosin contractions in the *C. elegans* spermatheca. Curr Biol 25, 141–151.
Totsukawa G, Wu Y, Sasaki Y, Hartshorne DJ, Yamakita Y, Yamashiro S, Matsumura F (2004). Distinct roles of MLCK and ROCK in the regulation of membrane protrusions and focal adhesion dynamics during cell migration of fibroblasts. J Cell Biol 164, 427–439.
Tse YC, Werner M, Longhini KM, Labbe J-C, Goldstein B, Glotzer M (2012). RhoA activation during polarization and cytokinesis of the early *Caenorhabditis elegans* embryo is differentially dependent on NOP-1 and CYK-4. Mol Biol Cell 23, 4020–4031.
Vicente-Manzanares M, Ma X, Adelstein RS, Horwitz AR (2009). Non-muscle myosin II takes centre stage in cell adhesion and migration. Nat Rev Mol Cell Biol 10, 778–790.
Ward JD (2015). Rapid and precise engineering of the *Caenorhabditis elegans* genome with lethal mutation co-conversion and inactivation of NHEJ repair. Genetics 199, 363–377.
Wettschureck N, Offermanns S (2002). Rho/Rho-kinase mediated signaling in physiology and pathophysiology. J Mol Med 80, 629–638.
Wiedemann N, Frazier AE, Pfanner N (2004). The protein import machinery of mitochondria. J Biol Chem 279, 14473–14476.
Wirshing ACE, Cram EJ (2017). Myosin activity drives actomyosin bundle formation and organization in contractile cells of the *Caenorhabditis elegans* spermatheca. Mol Biol Cell 28, 1937–1949.
Wirshing ACE, Cram EJ (2018). Spectrin regulates cell contractility through production and maintenance of actin bundles in the *Caenorhabditis elegans* spermatheca. Mol Biol Cell 29, 2433–2449.
Wissmann A, Ingles J, Mains PE (1999). The *Caenorhabditis elegans* mel-11 myosin phosphatase regulatory subunit affects tissue contraction in the somatic gonad and the embryonic epidermis and genetically interacts with the Rac signaling pathway. Dev Biol 209, 111–127.
Wissmann A, Ingles J, McGhee JD, Mains PE (1997). *Caenorhabditis elegans* LET-502 is related to Rho-binding kinases and human myotonic dystrophy kinase and interacts genetically with a homolog of the regulatory subunit of smooth muscle myosin phosphatase to affect cell shape. Genes Dev 11, 409–422.
Wong H-S, Dighe PA, Mezera V, Monternier P-A, Brand MD (2017). Production of superoxide and hydrogen peroxide from specific mitochondrial sites under different bioenergetic conditions. J Biol Chem 292, 16804–16809.
Xu Q, Huff LP, Fujii M, Griendling KK (2017). Redox regulation of the actin cytoskeleton and its role in the vascular system. Free Radic Biol Med 109, 84–107.
Xu S, Chisholm AD (2014). C. elegans epidermal wounding induces a mitochondrial ROS burst that promotes wound repair. Dev Cell 31, 48–60.
Yanase S, Onodera A, Tedesco P, Johnson TE, Ishii N (2009). SOD-1 deletions in *Caenorhabditis elegans* alter the localization of intracellular reactive oxygen species and show molecular compensation. J Gerontol Ser A Biol Sci Med Sci 64A, 530–539.